Self-Organization of a Mesoscale Bristle into Ordered, Hierarchical Helical Assemblies

Boaz Pokroy, *et al.*
Science **323**, 237 (2009);
DOI: 10.1126/science.1165607

ricate percolating semiconducting arrays. We propose that, in the low concentration regime ($c < 0.02$), cycloaddition provides an effective method to anchor molecules to the carbon nanotube framework and to either eliminate or transform metallic tubes. The data presented here suggest that $c \sim 0.018$ fluorination level is sufficient to achieve the complete conversion of the metallic tubes without degrading the semiconducting tubes. The latter is a necessary step for the production of semiconducting inks suitable for printable electronics. While the cycloaddition reaction provides the anchoring sites, the long, highly fluorinated side chains are quite effective in exfoliating the ropes, thus enabling the effective conversion of M-SWNT even deep inside the ropes, as is necessary for achieving high-performance devices. We demonstrated the utility of the method by fabricating TFTs using percolating arrays of functionalized carbon nanotubes as the semiconducting layer with mobilities of 100 cm^2/Vsec and on/off ratios of 10^5.

References and Notes

1. P. Avouris, Z. Chen, V. Perebeinos, *Nat. Nanotechnol.* **2**, 605 (2007).
2. E. S. Snow, P. M. Campbell, M. G. Ancona, *Appl. Phys. Lett.* **86**, 033105 (2005).
3. E. S. Snow *et al.*, *J. Vac. Sci. Technol. B* **22**, 1990 (2004).
4. E. Artukovic, M. Kaempgen, D. S. Hecht, S. Roth, G. Gruner, *Nano Lett.* **5**, 757 (2005).
5. H. Peng, N. T. Alvarez, C. Kittrell, R. H. Hauge, H. K. Schimdt, *J. Am. Chem. Soc.* **128**, 8396 (2006).
6. M. S. Arnold, A. A. Gree, J. F. Hulvat, S. I. Stupp, M. C. Hersam, *Nat. Mater.* **1**, 60 (2006).
7. P. G. Collins, M. S. Arnold, P. Avoris, *Science* **292**, 706 (2001).
8. M. S. Strano *et al.*, *Science* **301**, 1519 (2003).
9. J. Zhao, H. Park, J. Han, J. P. Lu, *J. Phys. Chem. B* **108**, 4227 (2004).
10. H. Park, J. Zhao, J. P. Lu, *Nano Lett.* **6**, 916 (2006).
11. R. Mclean, W. Huang, C. Khripin, A. Jogota, M. Zheng, *Nano Lett.* **6**, 55 (2006).
12. C. LeMieux *et al.*, *Science* **321**, 101 (2008).
13. Z. Chen, K. J. Ziegler, J. Shaver, R. H. Hauge, R. E. Smalley, *J. Phys. Chem. B* **110**, 11624 (2006).
14. E. S. Snow, J. P. Novak, P. M. Campbell, D. Park, *Appl. Phys. Lett.* **82**, 2145 (2003).
15. X.-Z. Bo *et al.*, *Appl. Phys. Lett.* **87**, 203510 (2005).
16. J. Zhao, Z. Chen, Z. Zhou, H. Park, P. R. Schyler, J. P. Lu, *Chem. Phys. Chem.* **6**, 598 (2005).
17. M. V. Veloso, A. G. Souza Filho, J. Mendes Filho, S. B. Fagan, R. Mota, *Chem. Phys. Lett.* **430**, 71 (2006).
18. Y.-S. Lee, N. Marzari, *J. Phys. Chem. C* **112**, 4480 (2008).
19. Y.-S. Lee, N. Marzari, *Phys. Rev. Lett.* **97**, 116801 (2006).
20. K. A. Park, Y. S. Choi, C. Kim, Y. H. Lee, *Phys. Rev. B* **68**, 045429 (2003).
21. J. Lu *et al.*, *J. Phys. Chem. B* **110**, 5655 (2006).
22. K. Kamaras, M. E. Itkis, H. Hu, B. Zhao, R. C. Haddon, *Science* **301**, 1501 (2003).
23. H. Hu *et al.*, *J. Am. Chem. Soc.* **125**, 14893 (2003).
24. C. Menard-Moyon, N. Izard, E. Doris, C. Mioskowski, *J. Am. Chem. Soc.* **128**, 6552 (2006).
25. K. S. Kim *et al.*, *Adv. Mater.* **14**, 1818 (2002).
26. K. H. An *et al.*, *Appl. Phys. Lett.* **80**, 4235 (2002).
27. H. F. Bettinger, K. N. Kudin, G. E. Scusseria, *J. Am. Chem. Soc.* **123**, 12849 (2001).
28. C.-M. Yang *et al.*, *Phys. Rev. B* **73**, 075419 (2006).
29. N. Nair, W.-J. Kim, M. L. Usrey, M. S. Strano, *J. Am. Chem. Soc.* **129**, 3946 (2007).
30. C. Wang *et al.*, *J. Am. Chem. Soc.* **127**, 11460 (2005).
31. Materials and methods are available as supporting material on *Science* Online.
32. J. Vavro, J. M. Kikkawa, J. E. Fischer, *Phys. Rev. B Condens. Matter* **71**, 155410 (2005).
33. A. Hagen, G. Moos, V. Talalaev, T. Hertel, *Appl. Phys. A* **78**, 1137 (2004).
34. J. Chen *et al.*, *Science* **282**, 95 (1998).
35. M. S. Dresselhaus, G. Dresselhaus, R. Saito, *Phys. Rep.* **409**, 47 (2005).
36. Supported by Air Force grant FA9550-071-0411. We thank H. L. Stormer and G. D. Jaycox for careful reading of the manuscript; R. Wheland for many interesting discussions; and D. Walls, J. Wyre, and N. G. Tassi for Raman, x-ray photoelectron spectroscopy, and high-resolution AFM inset at $c = 0.038$, respectively.

Self-Organization of a Mesoscale Bristle into Ordered, Hierarchical Helical Assemblies

Boaz Pokroy, Sung H. Kang, L. Mahadevan, Joanna Aizenberg*

Mesoscale hierarchical helical structures with diverse functions are abundant in nature. Here we show how spontaneous helicity can be induced in a synthetic polymeric nanobristle assembling in an evaporating liquid. We use a simple theoretical model to characterize the geometry, stiffness, and surface properties of the pillars that favor the adhesive self-organization of bundles with pillars wound around each other. The process can be controlled to yield highly ordered helical clusters with a unique structural hierarchy that arises from the sequential assembly of self-similar coiled building blocks over multiple length scales. We demonstrate their function in the context of self-assembly into previously unseen structures with uniform, periodic patterns and controlled handedness and as an efficient particle-trapping and adhesive system.

Non-centrosymmetric chiral, coiled, and spiral configurations are ubiquitous in nature, spanning from amino acids to mollusk shells to galaxies (*1*). On a mesoscopic scale, such structures are abundant in biology, and these are usually composed of helical fibers that are often further assembled into higher-order hierarchical materials. Natural examples include DNA helices, amyloid fibers (*2*), cellulose fibrils in wood (*3*), hierarchy in bone (*4, 5*), and chirally

spinning nodal cilia (*6*), to name a few, with implications on a variety of functions from information transfer to mechanical integrity and control of the body symmetry in morphogenesis. Man-made coiled and spiral materials and designs on a macroscopic scale are widely used in our everyday life—from ropes and bolts to helicopter rotors. On the molecular scale, chirality plays a critical role in asymmetric chemical synthesis and catalysis (*7*), liquid crystals (*8*), supramolecular chemistry (*9, 10*), and organic and inorganic crystal engineering (*11*). Artificial coiled structures at the mesoscale are rare, and these usually have simple geometries of one-dimensional helical fibers and ribbons (*1, 8–10, 12*). At any length scale, twist and handedness in superstructures gener-

ally originate from either the assembly of non-centrosymmetric building blocks or the application of a chiral field or template (*1–5, 8–13*). Here we report on the induction of capillarity-driven self-organization of a nanobristle into helical clusters and demonstrate the fabrication of non-trivial, hierarchically assembled, coiled meso-structures over large areas, in which neither the assembling elements nor the environment are chiral, guided by and consistent with simple theoretical considerations.

Our approach is presented in Fig. 1A. We consider a periodic array of nanopillars, each of which is anchored at one end on a substrate and free at the other. A locally stable configuration of the bristles is just a uniform array of non-interacting straight pillars (first-order structures). However, this is not necessarily a globally stable state: When the array is immersed in a liquid that is then evaporated, capillary forces associated with the liquid/vapor menisci between the free ends of the geometrically soft bristles may cause them to deform laterally and adhere to each other. The effect of elastocapillary coalescence (*14*) has been described for a well-known phenomenon of clumping in wet hair (*15*) or paintbrush immersed in paint (*16*). Similar clustering behavior is observed in nature in the examples of the tarsi of beetles (*17*) and spiders (*18*). The morphology and dynamics of the ensuing structures are a result of the competition between intrapillar elasticity and interpillar adhesion (*14–16*). Individual pillars that are long enough can bend easily to accommodate the capillary forces associated with the menisci between adjacent pillars.

School of Engineering and Applied Sciences, Wyss Institute for Biologically Inspired Engineering, Harvard University, Cambridge, MA 02138, USA.

*To whom correspondence should be addressed. E-mail: jaiz@seas.harvard.edu

A simple scaling analysis allows us to construct a set of rough criteria for the existence of these structures, in terms of the properties of the elastic circular nanopillars of radius r, length L, interpillar distance d, Young's modulus E, bending stiffness $B \sim Er^4$, and adhesive energy per unit area J (19) as well as the properties of the evaporating liquid of interfacial tension γ, in which they are immersed. Assuming that the pillars do not break through the meniscus, the longitudinal forces due to the pinned contact line cause the pillars to buckle (14); however, because the pillars have a circular cross section, there is no preferred plane of buckling. In addition, the multiple pinned menisci attract each other via a weak capillary interaction mediated by the interface (20). For the pillars to come together, the force $F_B \sim Bd/L^3$ to bend two adjacent pillars until they are just in contact at their tips must be comparable to the capillary force $F_C \sim \gamma r$ due to the menisci connecting the hemispherical ends. This yields a critical pillar length $L_c \sim (Bd/\gamma r)^{1/3} \sim (Ed/\gamma)^{1/3} r$, below which capillary forces will be unable to maintain a bent configuration and the bent pillars return to their upright state once the liquid has evaporated
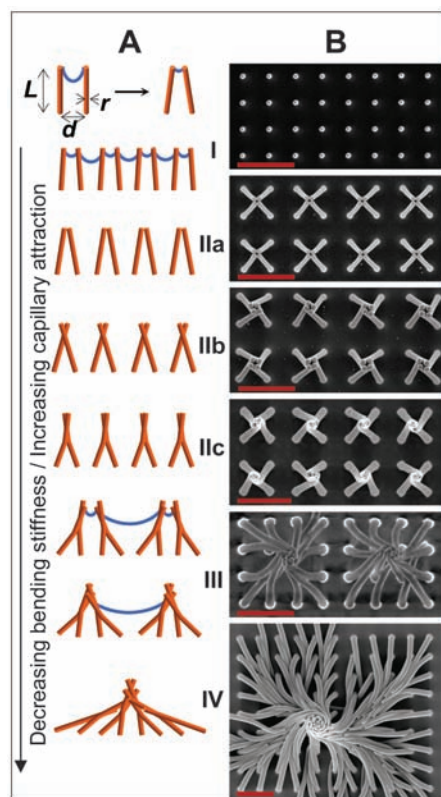
(regime I). When $L > L_c$, two neighboring pillars can retain contact as long as they are held together by either capillary forces or short-range van der Waals forces (after drying). A different characteristic length scale, $L_a \sim (Ed/J)^{1/3} r$, based on interpillar adhesion dictates whether the pillars will stay in their adhered state once capillary forces bring them together; for instance, if $L_a > L_c$ and $L_a > L > L_c$, the pillars will come together during the drying process but then separate eventually, corresponding to regime I. (These length scales may be modified by the wettability of the pillars, a detail that we will not discuss further here). When $L > L_c$ and $L \geq L_a$, we expect the pillars to form second-order stable clusters that usually reflect the symmetry of the underlying lattice (regime IIa). When $L \gg L_a$, the filaments can cluster to increase their adhesive contact via a chiral rearrangement of the pillars (regime IIb) and eventually twist around each other (regime IIc).

To understand this in a minimal model, we consider the adhesion of two initially straight free pillars (21) wound around each other along uniform helices of pitch p and radius R (19). Adhesive contact can now occur over a patch of approximately constant width a that winds around each filament and is determined by the solution of a JKR-like problem (22), yielding $a \sim (J/E)^{1/3} r^{2/3}$ [up to logarithmic factors of the form $\ln(L/r)$]. Then the total energy of two pillars of length L is the sum of the adhesive energy and the elastic energy (assumed to be caused by bending alone) and can be written as $U \sim -JaL(1 + 1/P^2)^{1/2} + BL/R^2(1 + P^2)^2$, where $P = p/2\pi R$. Here, the first
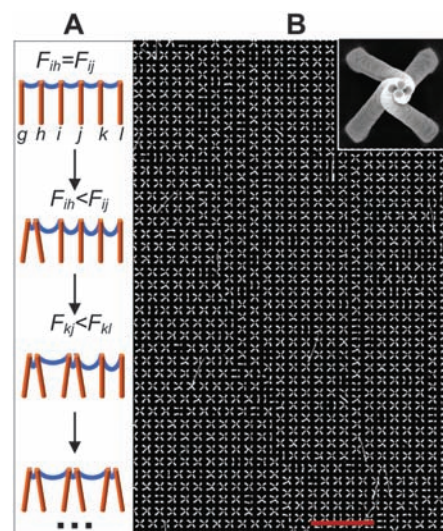
term corresponds to the energy of adhesion between two helices, whereas the second term corresponds to the elastic energy required to deform a naturally straight filament into a helix (23). For relatively stiff pillars, when $B/JaR^2 > 1$, it is evident that the minimum energy solution favors $P \to \infty$ (i.e., straight pillars); whereas for soft pillars, when $B/JaR^2 \leq 1$, minimizing U requires that the dimensionless pitch be as small as possible, which may be achieved by having $R \sim r$, $P \sim O(1)$ [i.e., a tightly wound helical configuration maximizing the length of contact between the filaments and corresponding to a second-order cluster (regime IIc)]. For pillars that have rotationally symmetric circular cross sections and are driven by a homogeneously drying front, the chirality of an individual cluster should be random. However, any asymmetry in the pillar cross section, pillar orientation, or the direction of the drying front can clearly lead to a specific handedness in the pattern. In any event, these helical clusters will then interact via the meniscus-driven capillary field to form higher-order coiled assemblies (III, IV,…) until the growing assembly is eventually halted by the elastic field that penalizes large deformations (15).

To test these ideas, we studied the evaporation-induced self-assembly in a square array of epoxy nanopillars fabricated as described previously (24). Droplets of wetting liquids (including anhydrous ethanol, isopropyl alcohol, anhydrous toluene, acetone, and mixtures of ethanol and water at different ratios) were placed on horizontally oriented substrates ($d = 2$ μm, $r = 150$ nm, $L = 4$ to 9 μm, $E = 0.1$ to 2 GPa, and controlled wall roughness) and were allowed to evaporate at ambient conditions. The evaporation-induced interactions and self-organization of the bristle were studied with the use of optical microscopy (Leica DMRX connected to a QImaging Evolution VF cooled color CCD camera) and a field emission scanning electron microscope (Zeiss Ultra 55).

The resulting structures were in substantial agreement with the simple theory sketched above, and all of the predicted structures—from the first-order unclustered nanobristle to the fourth-order helical bundles—were observed (Fig. 1B). By using a periodic square array of nanopillars, we achieved a long-range order in the assembled bristle, such that large-area (up to millimeters), uniform domains of highly periodic bundles were generated from the nanometer-sized building blocks. Figure 2A and movie S1 illustrate the mechanism for the propagation of order in the array of the assembling pillars. When the liquid evaporates to the level of the free tips, a meniscus connecting the neighboring pillars is formed. In an equally spaced array, the lateral capillary forces acting on each pillar are fully balanced, and no lateral movement occurs. However, imperfections and instabilities, which include local differences in the evaporation rate, pinning of the contact line, and variations in the interpillar

Fig. 1. (**A**) Schematic diagrams and (**B**) corresponding scanning electron microscopy (SEM) images showing the morphogenesis of helical patterns, from the first-order unclustered nanobristle to the fourth-order coiled bundle. Scale bars, 4 μm. Note the hierarchical nature of the assembly reflected in the presence of the lower-order braids in the large clusters braided in a unique structure reminiscent of modern dreadlocks or mythical Medusa.

Fig. 2. Large-area self-organization of the bristle. (**A**) Schematic diagram showing the mechanism of the formation of the long-range order in the assembled bristle. See text for further details. (**B**) SEM image showing the assembly into uniform, periodic fourfold clusters of nanopillars over the submillimeter area. Note the different coherent domains that arise from the multiple nucleation sites. Scale bar, 20 μm.

lattice spacing, will nucleate the first pillar cluster at a particular location rather than randomly (for example, between pillars h and g). As a result, the next pillar i will sense an anisotropic force field where $F_{ih} < F_{ij}$ and will bend in the direction of the pillar j. This process will prop-
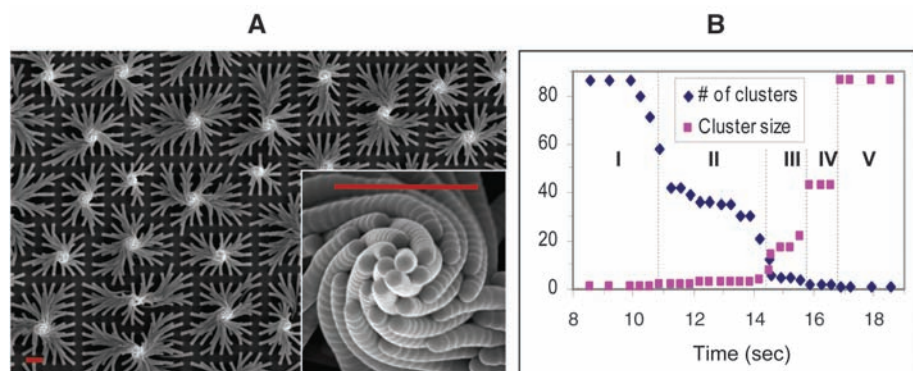

Fig. 3. Hierarchical assembly into large coiled clusters. (**A**) SEM showing an array of pillars ($L = 8$ μm) self-organized from the ethanol solution into the level IV and V helical assemblies. (Inset) Magnified view of the coiled core. Scale bars, 3 μm. (**B**) Kinetics of the hierarchical assembly. The growth of one representative cluster is shown. The number of clusters was monitored by analyzing the consecutive images from movie S2. The cluster size is defined as the number of pillars in the bundle. The multistep, sequential coalescence of the small blocks into higher-order structures is apparent. The y axis denotes the number or size of clusters.
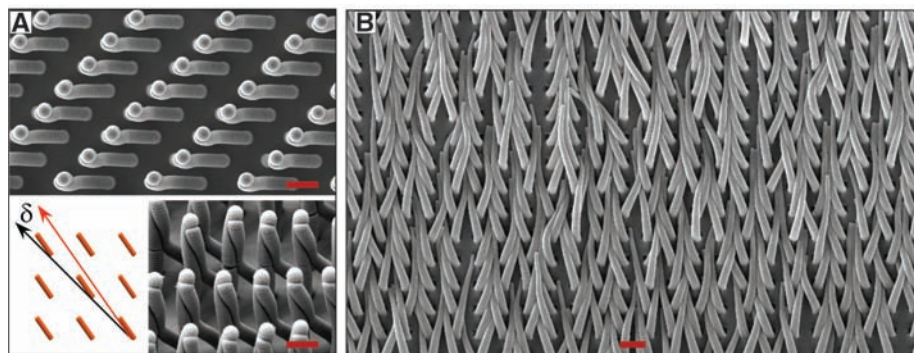

Fig. 4. Controlling handedness and pattern of assembled structures. (**A**) Top and angled SEM views showing an array of ordered helical pairs with uniform handedness. (Inset) Schematic diagram that illustrates the substrate design. The bristles were first tilted in the direction that forms a small angle δ with the principal diagonal direction of the underlying square lattice (shown by the red and black lines, respectively) and then allowed to assemble. (**B**) Evaporation along the surface results in the woven braids assembled parallel to the substrate. Scale bars, 2 μm.

Fig. 5. Illustration of the adhesive and particle-trapping potential of the helically assembling bristle. (**A**) Low-magnification SEM showing the capture of the 2.5-μm polystyrene spheres (indicated by arrows). Scale bar, 10 μm. (**B**) Magnified view depicting a single sphere trapped through the conformal wrapping of the nanobristle. Scale bar, 2 μm. (**C**) Coiled whirlpools remain after the removal of the spheres. Scale bar, 2 μm.
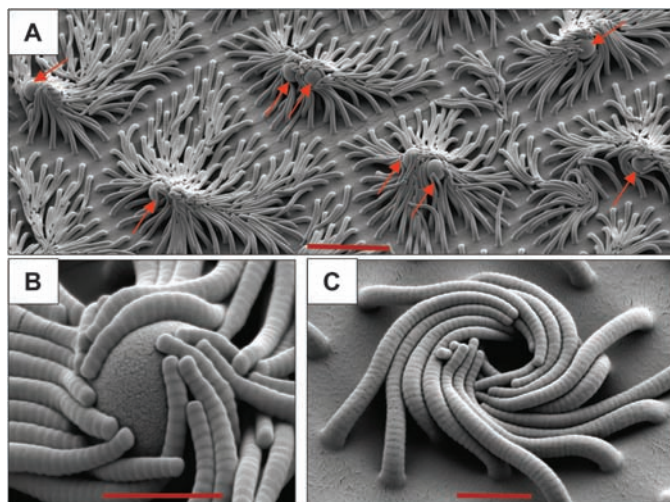
agate through the bristle and generate long-range ordered domains (Fig. 2A). For example, to bias the system to form periodic second-order bundles over a large area, we chose conditions that would lead solely to the formation of clusters of four bristles whose stiffness would not allow their further assembly into higher-order structures. Epoxy bristles with $E = 1$ GPa, $r = 150$ nm, $L = 5$ μm, and $d = 2$ μm immersed in ethanol as a wetting liquid satisfied this condition. Figure 2B shows a fragment of the corresponding assembled structure with the marked long-range order.

A detailed microscopy study shows that the cluster twisting is a dynamic, multistep process with distinctive kinetics and a growth mechanism that involves the sequential coalescence of self-similar coiled blocks to yield organized helical patterns on very large scales (Fig. 3 and movie S2). To achieve the formation of higher-order structures III to V, the nanopillars were specifically designed to have rough, banded walls. In addition to increasing flexibility, this segmented, "wormlike" geometry (Fig. 3A, inset) provides the pinning of the receding contact line by re-entrant curvature (25, 26) and, thus, an increase in the capillary attraction necessary to bring the larger clusters together. The history of the hierarchical assembly process is imprinted in the makeup of the final helical structures: The lower-order braids and bundles can be clearly identified in the larger coiled clusters (Figs. 1B, bottom, and 3). The kinetics of this multistep process are depicted in Fig. 3B.

Because the instabilities leading to the chiral rearrangement of the clustered pillars are random, a mixture of bundles with the right- and left-handed twist was observed. To optimize our system to achieve the uniform handedness of the clusters, we used two approaches to the bristle design. The pillars were either (i) rendered elliptical in cross section or (ii) an array of tilted pillars was used (24). The ellipses' axes or the tilt direction of the pillars were chosen to make a small angle with the principal unit cell directions in the underlying square lattice (Fig. 4A). Such a design induces an anisotropy in the stiffness of the bristle that results in a directional, off-axis bending of the pillars under the influence of the capillary forces and allows us to form an ordered array of helices with uniform controlled right- or left-handedness (Fig. 4A). This is similar in concept to the use of a pre-tilt layer in liquid crystal displays to bias otherwise vertically aligned nematic crystals and prevent the formation of defects during switching (27). Alternatively, the pattern and orientation of the assembled coiled bundles could also be orchestrated by changing the direction of the evaporation front. Figure 4B provides an example of the latter approach—a woven carpet composed of braids of nanopillars uniformly plaited parallel to the surface—that results from the evaporation front moving parallel to the substrate.

Recent studies show that the adhesive properties in a variety of biological systems arise

from the conformal attachment of microscopic fibers to surfaces and objects and their subsequent entanglement (*17*, *28*). The observed mechanical interlocking in our artificial, spirally assembling bristle can be used in a similar manner and may lead to an effective adhesive and particle-trapping system. Figure 5 shows microspheres that are captured through conformal wrapping and twisting of the nanobristle. The adhesion is extremely stable, and the particles remain attached even after rigorous sonication. The process is equally applicable for attaching to objects with arbitrary shapes and surfaces with various topographies.

Though lateral adhesion is known to occur in high–aspect ratio structures such as photoresists and soft lithographic stamps (*29*, *30*), arrays of carbon and ZnO nanotubes (*31*, *32*), and biomimetic setal adhesives (*33*), this process has been generally described as an unwanted outcome that leads to the uncontrolled collapse of the structures. The clustered features were usually irregular in size, and no order over the large area was observed unless templating was used (*34*). Here we have demonstrated that the process can, in fact, be finely tuned to yield organized nontrivial, helical assemblies with controlled size, pattern, hierarchy, and handedness over large areas. These mesoscale coiled structures may be useful in a number of applications: They have the ability to store elastic energy and information embodied in the adhesive patterns that can be created at will. Additionally, they may be used as an efficient adhesive or capture-and-release system, provide the foundation for hierarchically assembled structural materials, and be used to induce chiral flow patterns in the ambient flow and thus be applied for enhanced mixing and directed transport at the micron and submicron scale. These structures may serve as the seed for the spontaneous breaking of symmetry on large scales, just as chirally spinning cilia ultimately control the left-right asymmetry in vertebrate morphogenesis (*6*).

References and Notes

1. M. M. Green, R. J. M. Nolte, E. W. Meijer, *Materials-Chirality*, vol. 24 of *Topics in Stereochemistry*, S. E. Denmark, J. Siegel, Eds. (Wiley, Hoboken, NJ, 2003).
2. N. Rubin, E. Perugia, M. Goldschmidt, M. Fridkin, L. Addadi, *J. Am. Chem. Soc.* **130**, 4602 (2008).
3. H. Lichtenegger, M. Muller, O. Paris, C. Riekel, P. Fratzl, *J. Appl. Crystallogr.* **32**, 1127 (1999).
4. W. Wagermaier *et al.*, *Biointerphases* **1**, 1 (2006).
5. S. Weiner, H. D. Wagner, *Annu. Rev. Mater. Sci.* **28**, 271 (1998).
6. J. J. Essner *et al.*, *Nature* **418**, 37 (2002).
7. H. C. Kolb, M. S. Vannieuwenhze, K. B. Sharpless, *Chem. Rev.* **94**, 2483 (1994).
8. J. W. Goodby, *J. Mater. Chem.* **1**, 307 (1991).
9. E. D. Sone, E. R. Zubarev, S. I. Stupp, *Angew. Chem. Int. Ed.* **41**, 1705 (2002).
10. J. S. Moore, S. I. Stupp, *J. Am. Chem. Soc.* **114**, 3429 (1992).
11. T. E. Gier, X. H. Bu, P. Y. Feng, G. D. Stucky, *Nature* **395**, 154 (1998).
12. J. Zhu *et al.*, *Nat. Nanotechnol.* **3**, 477 (2008).
13. C. A. Orme *et al.*, *Nature* **411**, 775 (2001).
14. A. E. Cohen, L. Mahadevan, *Proc. Natl. Acad. Sci. U.S.A.* **100**, 12141 (2003).
15. J. Bico, B. Roman, L. Moulin, A. Boudaoud, *Nature* **432**, 690 (2004).
16. H. Y. Kim, L. Mahadevan, *J. Fluid Mech.* **548**, 141 (2006).
17. T. Eisner, D. J. Aneshansley, *Proc. Natl. Acad. Sci. U.S.A.* **97**, 6568 (2000).
18. O. Betz, G. Kolsch, *Arthropod Struct. Dev.* **33**, 3 (2004).
19. S. Neukirch, G. van der Heijden, *J. Elast.* **69**, 41 (2002).
20. M. M. Nicolson, *Proc. Cambridge Philos. Soc.* **45**, 288 (1949).
21. This is a simplification of the actual geometry of the pillars that are attached to a substrate at one end and free at the other. Yet, the case of free pillars that can bend, twist, and adhere is sufficient to understand the conditions when helical structures can arise. In the experimental setup, however, it is this broken symmetry induced by the attachment that leads to the observed complex braided structures of generalized helices of variable pitch and radius.
22. K. L. Johnson, *Contact Mechanics* (Cambridge Univ. Press, Cambridge, 1985).
23. For a pillar with a circular cross section, the twist of the cross section is a constant. Although adhesion can lead to twisting, because there is a lubricating layer of fluid between the pillars, we will assume that the pillars can bend without twisting as they wind around each other. The bending energy of a filament of length L is $U_b \sim B\kappa^2 L$. Therefore, for a helix of radius R and pitch p ($P = p/2\pi R$) that has curvature $\kappa = 1/R(1 + P^2)$, $U_b \sim BL/R^2(1 + P^2)^2$. For helically entwined pillars that are relatively straight (i.e., have a large pitch), the contact zone is straight and thus smaller than the pillar length (a consequence of the relative inextensibility of the pillars) and confers no energetic advantage. However, when the pitch of the tightly entwined pillars falls below a threshold, contact itself occurs over a helical patch (*19*) with a length that scales as $L(1 + 1/P^2)^{1/2}$, so that the adhesion energy $U_a \sim -JaL(1 + 1/P^2)^{1/2}$ increases as the pitch decreases further.
24. B. Pokroy, A. Epstein, M. C. M. Persson Gulda, J. Aizenberg, *Adv. Mater.*, published online 18 November 2008; 10.1002/adma.200801432.
25. A. Ahuja *et al.*, *Langmuir* **24**, 9 (2008).
26. A. Tuteja *et al.*, *Science* **318**, 1618 (2007).
27. P. J. Collings, M. Hird, *Introduction to Liquid Crystals* (Taylor and Francis, Bristol, UK, 1997).
28. K. Autumn *et al.*, *Nature* **405**, 681 (2000).
29. C. Y. Hui, A. Jagota, Y. Y. Lin, E. J. Kramer, *Langmuir* **18**, 1394 (2002).
30. Y. G. Y. Huang *et al.*, *Langmuir* **21**, 8058 (2005).
31. A. Dev, S. Chaudhuri, *Nanotechnology* **18**, 175607 (2007).
32. H. Liu, J. Zhai, L. Jiang, *Soft Matter* **2**, 811 (2006).
33. A. K. Geim *et al.*, *Nat. Mater.* **2**, 461 (2003).
34. A. Sidorenko, T. Krupenkin, A. Taylor, P. Fratzl, J. Aizenberg, *Science* **315**, 487 (2007).
35. This work was partially supported by the Materials Research Science and Engineering Center under NSF award no. DMR-0213805. We acknowledge the use of the facilities at the Harvard Center for Nanoscale Systems supported by NSF award no. ECS-0335765. B.P. is grateful to the Fulbright Visiting Scholar Program for financial support.

Historical Warnings of Future Food Insecurity with Unprecedented Seasonal Heat

David. S. Battisti[1] and Rosamond L. Naylor[2]

Higher growing season temperatures can have dramatic impacts on agricultural productivity, farm incomes, and food security. We used observational data and output from 23 global climate models to show a high probability (>90%) that growing season temperatures in the tropics and subtropics by the end of the 21st century will exceed the most extreme seasonal temperatures recorded from 1900 to 2006. In temperate regions, the hottest seasons on record will represent the future norm in many locations. We used historical examples to illustrate the magnitude of damage to food systems caused by extreme seasonal heat and show that these short-run events could become long-term trends without sufficient investments in adaptation.

The food crisis of 2006–2008 demonstrates the fragile nature of feeding the world's human population. Rapid growth in demand for food, animal feed, and biofuels, coupled with disruptions in agricultural supplies caused by poor weather, crop disease, and export restrictions in key countries like India and Argentina, have created chaos in international markets (*1*). Coping with the short-run challenge of food price volatility is daunting. But the longer-term challenge of avoiding a perpetual food crisis under conditions of global warming is far more serious. History shows that extreme seasonal heat can be detrimental to regional agricultural productivity and human welfare and to international agricultural markets when policy-makers intervene to secure domestic food needs.

We calculated the difference between projected and historical seasonally averaged temperatures (*2*) throughout the world by using output from the 23 global climate models contributing to the Intergovernmental Panel on Climate Change's (IPCC) 2007 scientific synthesis (*3*). Our results show that it is highly likely (greater than 90%

[1]Department of Atmospheric Sciences, University of Washington, Seattle, WA 98195–1640, USA. E-mail: battisti@washington.edu [2]Program on Food Security and the Environment, Stanford University, Stanford, CA 94305–6055, USA. E-mail: roz@stanford.edu